with ⟨100⟩ almost parallel to the column axis. Note that each columnar crystal contains many primary dendrite arms. As the diameter of these grains increases additional primary dendrite arms appear by a mechanism in which some tertiary arms grow ahead of their neighbours as shown in the figure.

The volume fraction of the melt solidified increases with increasing distance behind the tips of the dendrites and, when the structure is mainly single-phase, the secondary and tertiary arms of adjacent dendrites can link up to form walls of solid containing many primary dendrite arms. The region between the tips of the dendrites and the point where the last drop of liquid is solidifying is known as the *mushy* or *pasty* zone. The length of this zone depends on the temperature gradient and the non-equilibrium freezing range of the alloy. In general it is found that the secondary arms become coarser with distance behind the primary dendrite tips. This effect can be seen in Fig. 4.28. The primary and secondary dendrite arm spacing is also often found to increase with increasing distance from the mould wall. This is simply due to a corresponding decrease in the cooling rate with time after pouring.

Equiaxed Zone

The equiaxed zone consists of equiaxed grains randomly oriented in the centre of the ingot. An important origin of these grains is thought to be melted-off dendrite side-arms. It can be seen from Fig. 4.28 that the side-arms are narrowest at their roots. Therefore, if the temperature around the dendrite increases after it has formed, it will begin to melt and may become detached from the main stem. Provided the temperature falls again before the arm completely disappears it can then act as a 'seed' for a new dendrite. An effective source of suitable temperature pulses is provided by the turbulent convection currents in the liquid brought about by the temperature differences across the remaining melt. Convection currents also provide a means of carrying the melted-off arms away to where they can develop uninhibited into equiaxed dendrites. If convection is reduced fewer seed crystals are created causing a larger final grain size and a greater preponderance of columnar grains. Convection also plays a dominant role in the formation of the outer chill zone. The mechanism whereby crystals are melted away from the mould walls is thought to be similar to the detachment of side-arms[15] and when convection is absent no chill zone is observed.

Shrinkage Effects

Most metals shrink on solidification and this has important consequences for the final ingot structure. In alloys with a narrow freezing range the mushy zone is also narrow and as the outer shell of solid thickens the level of the remaining liquid continually decreases until finally when solidification is complete the ingot contains a deep central cavity or *pipe*.

In alloys with a wide freezing range the mushy zone can occupy the whole of the ingot. In this case no central pipe is formed. Instead the liquid level gradually falls across the width of the ingot as liquid flows down to compensate for the shrinkage of the dendrites. However, as the interdendritic channels close up this liquid flow is inhibited so that the last pools of liquid to solidify leave small voids or pores.

4.4.2 Segregation in Ingots and Castings

Two types of segregation can be distinguished in solidified structures. There is *macrosegregation*, i.e. composition changes over distances comparable to the size of the specimen, and there is *microsegregation* that occurs on the scale of the secondary dendrite arm spacing.

It has already been shown that large differences in composition can arise across the dendrites due to coring and the formation of non-equilibrium phases in the last solidifying drops of liquid. Experimentally it is found that while cooling rate affects the spacing of the dendrites it does not substantially alter the amplitude of the solute concentration profiles provided the dendrite morphology does not change and that diffusion in the solid is negligible. This result often applies to quite a wide range of practical cooling rates.

There are four important factors that can lead to macrosegregation in ingots. These are: (i) shrinkage due to solidification and thermal contraction; (ii) density differences in the interdendritic liquid: (iii) density differences between the solid and liquid; and (iv) convection currents driven by temperature-induced density differences in the liquid. All of these factors can induce macrosegregation by causing mass flow over large distances during solidification.

Shrinkage effects can give rise to what is known as *inverse segregation*. As the columnar dendrites thicken solute-rich liquid (assuming $k < 1$) must flow back between the dendrites to compensate for shrinkage and this raises the solute content of the outer parts of the ingot relative to the centre. The effect is particularly marked in alloys with a wide freezing range, e.g. Al–Cu and Cu–Sn alloys.

Interdendritic liquid flow can also be induced by gravity effects. For example during the solidification of Al–Cu alloys the copper rejected into the liquid raises its density and causes it to sink. The effect can be reinforced by convection currents driven by temperature differences in the ingot.

Gravity effects can also be observed when equiaxed crystals are forming. The solid is usually denser than the liquid and sinks carrying with it less solute than the bulk composition (assuming $k < 1$). This can, therefore, lead to a region of negative segregation near the bottom of the ingot.

The combination of all the above effects can lead to complex patterns of macrosegregation. Fig. 4.43 for example illustrates the segregation patterns found in large steel ingots[16].

In general segregation is undesirable as it has marked deleterious effects on mechanical properties. The effects of microsegregation can be mitigated by subsequent homogenization heat treatment, but diffusion in the solid is far too

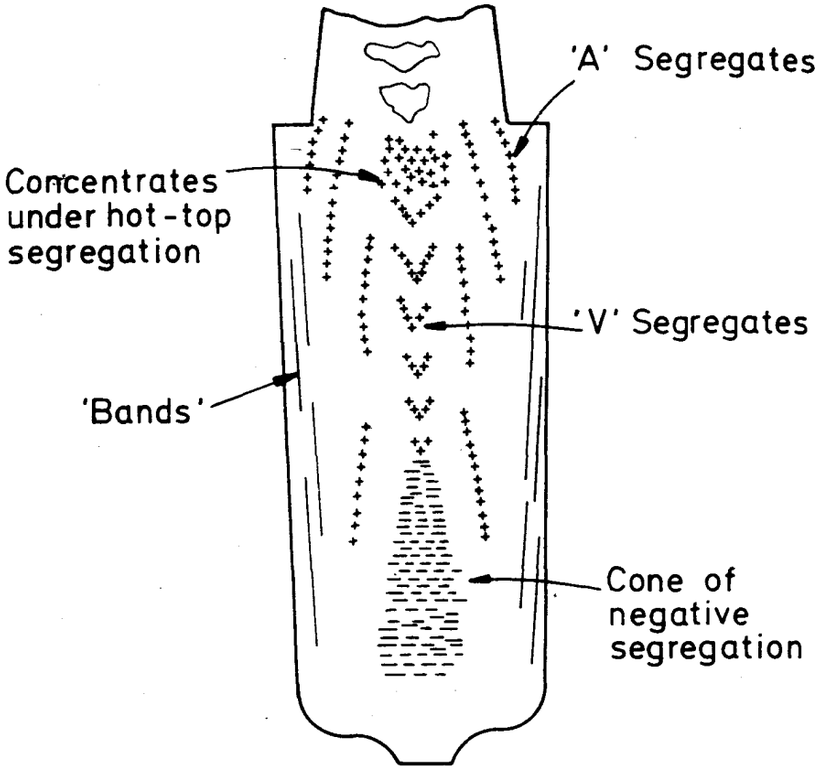

Fig. 4.43 Segregation pattern in a large killed steel ingot. + positive, − negative segregation. (After M.C. Flemings, *Scandinavian Journal of Metallurgy* **5** (1976) 1.)

slow to be able to remove macrosegregation which can only be combated by good control of the solidification process.

4.4.3 *Continuous Casting*

A number of industrial processes are nowadays employed in which casting is essentially a dynamic rather than a static process. In these cases, the molten metal is poured continuously into a water-cooled mould (e.g. copper) from which the solidified metal is continuously withdrawn in plate or rod form. This process is illustrated schematically in Fig. 4.44.

It is seen that the speed of withdrawal is such that the solid–liquid interface is maintained in the shape and position illustrated. Ideally, the flow behaviour of the liquid should be vertically downwards, and if flow is maintained in this way the final composition across the ingot will be kept uniform. In practice,

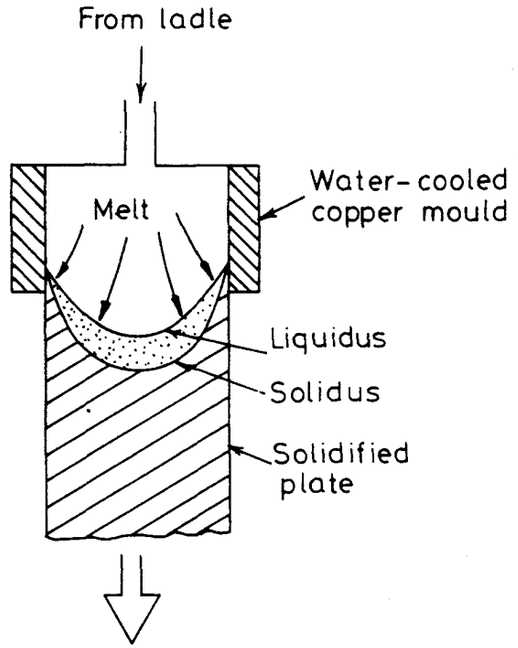

Fig. 4.44 Schematic illustration of a continuous casting process.

hydrodynamic effects do not allow this simple type of flow and there is a tendency for the flow lines to fan outwards (as shown by the arrows) producing negative segregation near the centre. Solidification follows the maximum temperature gradient in the melt as given by the normals to the isotherms. In certain respects weld solidification has much in common with continuous casting in that it is also a dynamic process. As illustrated in Fig. 4.45 the main difference is of course that in continuous casting the heat source (as defined by the mould) does not move, whereas in welding the heat source (the electrode) is moving. We shall now consider the latter case in more detail, but it will be found that certain conclusions concerning weld solidification behaviour can well be applied to both processes.

Heat Flow in Welding and Continuous Casting

As discussed earlier, there are many factors concerning heat distribution at the melt zone and the dynamics of the process, which are essentially fairly similar in both continuous casting and welding. As an example we shall first consider the welding process and then discuss how the results may be applied to continuous casting. In contrast to continuous casting, weld solidification involves a 'mould' that has approximately the same composition as the melt.

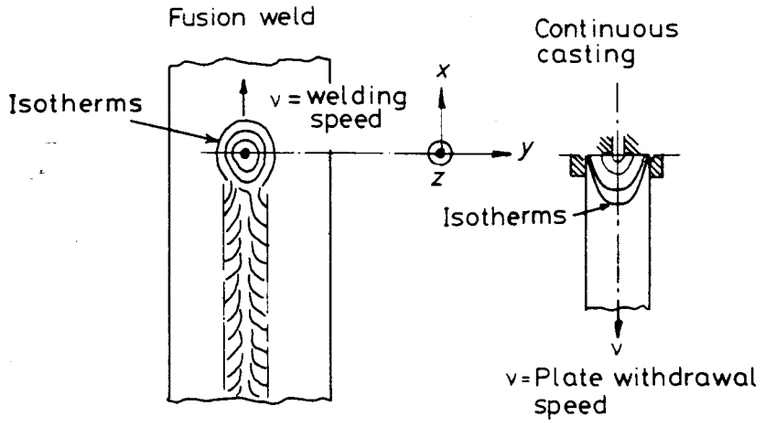

Fig. 4.45 Illustrating the essential equivalence of isotherms about the heat sources in fusion welding and continuous casting.

The most important variables in weld solidification or continuous casting are thus:

1. The rate of heat input, q (determined by type of weld process, weld size, etc.); in terms of continuous casting q is represented effectively by the volume and temperature of the melt.
2. Speed of arc movement along join, v; in continuous casting, v is the velocity of plate withdrawal.
3. Thermal conductivity of the metal being welded or cast, K_s.
4. Thickness of plate being welded or cast, t.

In the case of welding, assuming that the arc moves along the x coordinate, the resulting heat distribution in a three-dimensional solid plate is given by the solution to the heat flow equation[19]:

$$\frac{\partial^2 T}{\partial x^2} + \frac{\partial^2 T}{\partial y^2} + \frac{\partial^2 T}{\partial z^2} = 2K_s v \frac{\partial T}{\partial (x - vt)} \tag{4.47}$$

where x, y, z are defined in Fig. 4.45 and t is time.

Solving this equation gives the temperature distribution about the moving heat source in the form of isotherms in the solid metal, in which the distance between the isotherms in a given direction (x, y, z) is approximately given by:

$$\lambda_{(x,y,z)} \propto \frac{q}{K_s v t} \tag{4.48}$$

Gray *et al.* (1975) have solved Equation 4.47 and plotted isotherms for a number of different materials and welding speeds and some of their results are summarized in Fig. 4.46.

Assuming a similar isotherm distribution in the melt, it is likely that the

parameters K_s, v, t and q will largely determine solidification morphology, in that dendrites always try to grow in directions as near normal to isotherms as their crystallography allows. It is seen in the above figure, for example, that holding q, v and t constant (Fig. 4.46a), the distance between isotherms, λ, increases substantially as a function of the change of heat conductivity, K_s, of the different materials: aluminium, carbon (ferritic) steel, and austenitic steel. If the plate thickness is increased (Fig. 4.46b), or the weld speed is higher (Fig. 4.46c), λ also decreases proportionally.

These results can also be applied to *continuous casting*, in that the isotherm distributions shown in Fig. 4.46 are affected in a similar way by the conductivity of the solidifying metal and its speed of withdrawal from the mould. This means, for example, that the depth of the liquid pool in continuous casting is much greater for steel than for aluminium alloys under comparable condi-

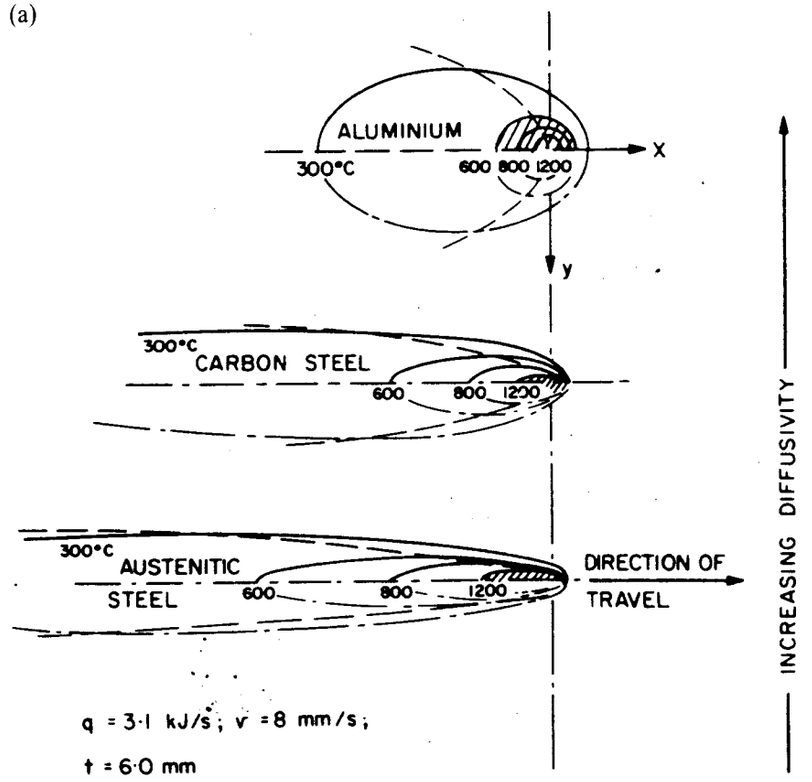

Fig. 4.46 Effect of various parameters in Equation 5.36 on the isotherm distribution at a point heat source. (a) Effect of changes in thermal conductivity, K_S. (b) Effect of changes in plate thickness, t. (c) Effect of changes in movement of heat source, v. (After T.G. Gray, J. Spence and T.H. North, *Rational Welding Design*, Newnes-Butterworth, London, 1975.)

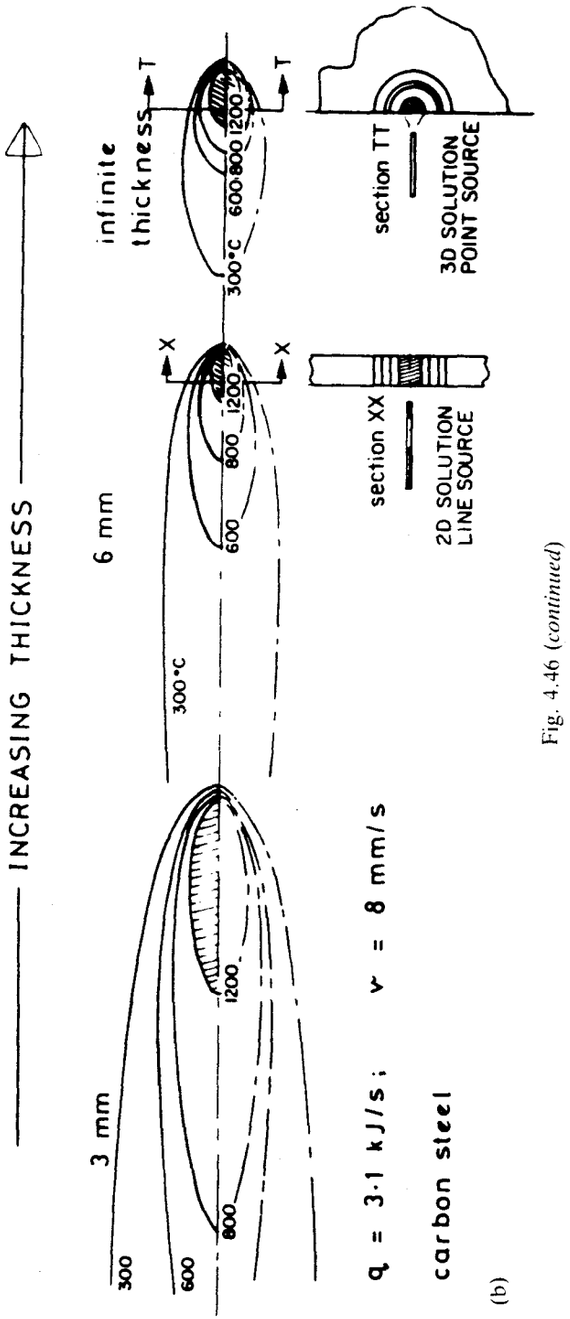

Fig. 4.46 (*continued*)

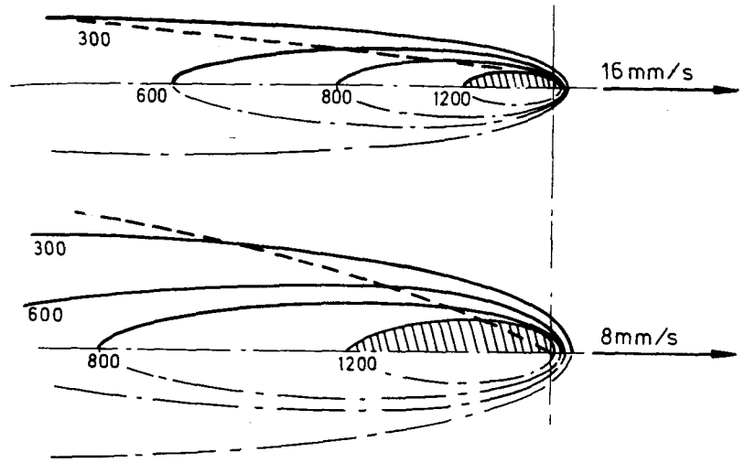

Fig. 4.46 (*continued*)

tions. This implies that in practice the maximum casting speed and billet cross-section are less for steel than for aluminium or copper. Another practical difficulty resulting from a large depth of liquid is that the billet can not be cut until it reaches a point well beyond the solidus line (see Fig. 4.44), which requires in fact a very tall installation for high speed casting.

4.5 Solidification of Fusion Welds

Contact between the weld melt and the base metal will initially cause melting back of the base material and dilution of the filler metal as illustrated in Fig. 4.47. The amount of dilution involved is not insignificant. Jesseman (1975)[17] reports for example that in microalloyed steel welds, the weld metal may contain 50–70% of the amount of Nb, Ti or V as analysed in the base material. The effect of dilution is in fact threefold, and affects the weld metal

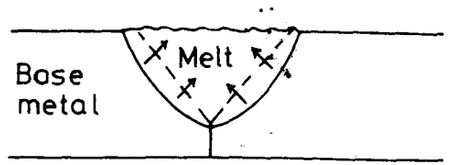

Fig. 4.47 Illustrating the effect of dilution. In high-energy welds, the weld metal typically exhibits 50–70% of the analysis of microalloying elements of the base metal through dilution.

as follows:

1. The composition of the melt is changed.
2. The surface oxide layer of the base metal is removed (also into the melt).
3. It cools down the melt.

Depending upon the type of material being welded as well as plate thickness, the base metal behaves as a very efficient heat sink, and already at $T \simeq T_e$ solidification nuclei form at the oxide-free surface of the melted-back base material. Since the melt has approximately the same composition as the base metal, 'wetting' of the base metal is very efficient and $\theta \simeq 0$ (see Fig. 4.7). This implies in turn that there is almost no nucleation barrier to solidification and hence very little undercooling occurs. Solidification is thus predicted to occur epitaxially, i.e. nuclei will have the same lattice structure and orientation as the grains at the solid–liquid surface of the base metal, and this is what is observed in practice.

Since the temperature of the melt beneath the arc is so high and the base material is such an efficient heat sink there is initially a steep temperature gradient in the liquid and consequently the degree of constitutional supercooling is low. The actual thermal gradient is of course dependent upon the welding process and the plate thickness (Equation 4.48). For example TIG welding of thin plates will give steeper thermal gradients than submerged arc

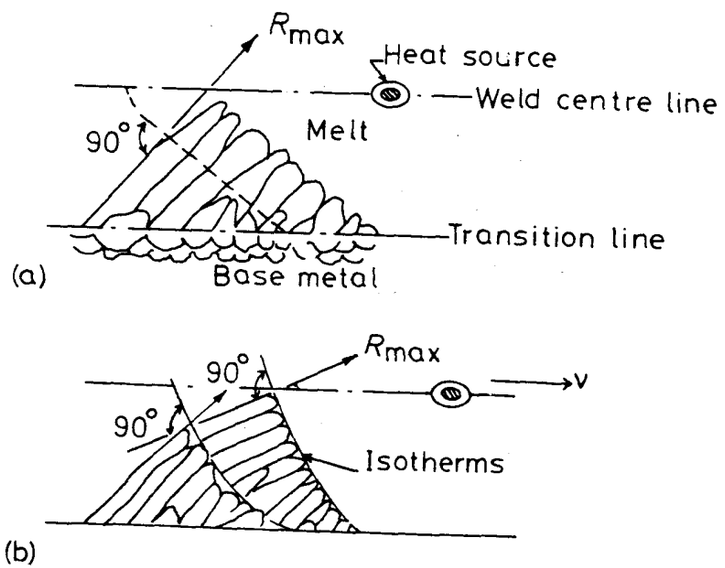

Fig. 4.48 Illustrating the growth of columnar crystals in the weld, and how growth continues to occur approximately normal to the isotherms.

welding of thick plates, the latter process having the higher heat input. Since certain grains at the base metal are better oriented than others for ⟨100⟩ growth with respect to the isotherms of the melt, these quickly predominate and widen at the expense of the others. However, the general coarseness of the microstructure is largely determined at this stage by the grain size of the base metal. Unfortunately, the base metal at the transition zone receives the most severe thermal cycle and after high-energy welding in particular the grains in this zone tend to grow and become relatively coarse. The weld microstructure is thus inherently coarse grained.

Welding is essentially a dynamic process in which the heat source is continuously moving. This means that the maximum temperature gradients are constantly changing direction as the heat source moves away. The growing columnar crystals are thus faced with the necessity of trying to follow the maximum temperature gradients while still maintaining their preferred ⟨100⟩ growth direction. This often results in sudden changes in growth direction, as illustrated in Fig. 4.48a and b.

Few of the grains originating at the base metal survive to reach the weld centre line. The mechanism by which sudden changes in ⟨100⟩ growth direction are brought about is not fully understood. One suggestion is that renucleation occurs by the help of dendritic fragments which have broken away from the growing interface due to turbulence in the weld pool, or simply from melted-off dendrite arms.

Influence of Welding Speed

An important effect of increasing the welding speed is that the shape of the weld pool changes from an elliptical shape to a narrower, pear shape (see,

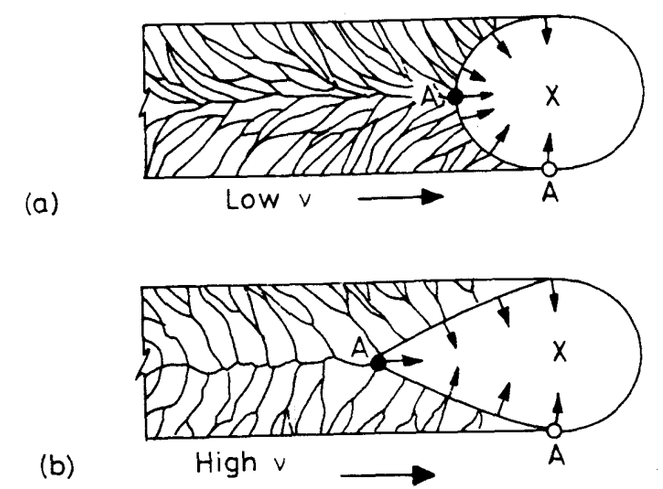

Fig. 4.49 Illustrating the effect of increasing welding speed on the shape of the melt pool and crystal growth in fusion welds.

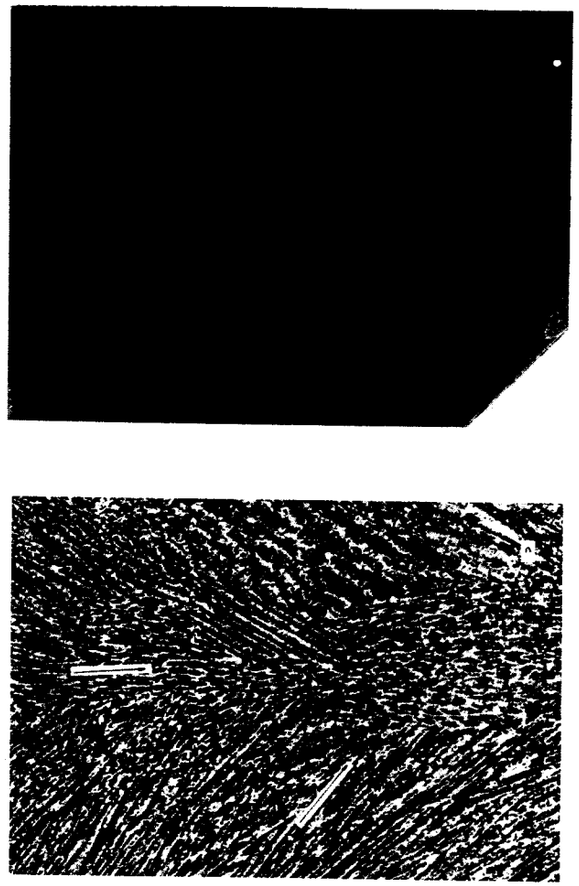

Fig. 4.50 (a) TIG weld of nickel, illustrating low crystal growth speed × 25 (by Gudrun Keikkala, University of Luleå, Sweden). (b) Submerged arc weld of steel, illustrating high growth speed × 24 (by H. Åström, University of Luleå, Sweden).

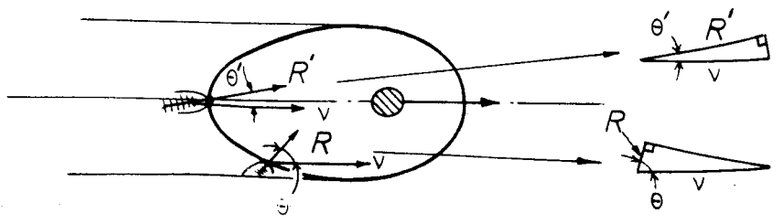

Fig. 4.51 Illustrating the relationship between crystal growth speed and welding speed in terms of rate vectors.

e.g. Fig. 4.49). Since growing crystals try to follow the steepest temperature gradients, the effect of changing the welding speed is to alter the solidification behaviour as illustrated in Fig. 4.49. As shown in 4.49b, the pear-shaped weld pool maintains fairly constant thermal gradients up to the weld centre-line, corresponding to the more angular geometry of the melt in this case. On this basis growing crystals are not required to change growth direction as at slower speeds (Fig. 4.49a). Instead, appropriately oriented crystals stabilize and widen outgrowing crystals of less favourable orientation. The crystal morphology shown in Fig. 4.49b is in fact fairly typical of the high production rate welds based on modern submerged arc welding. An example of a submerged arc weld is shown in Fig. 4.50b, and of a TIG weld of nickel in 4.50a.

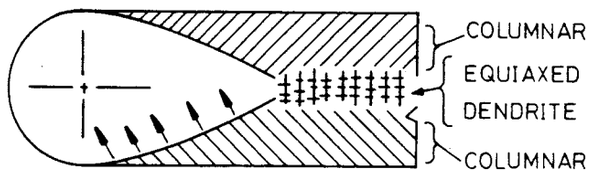

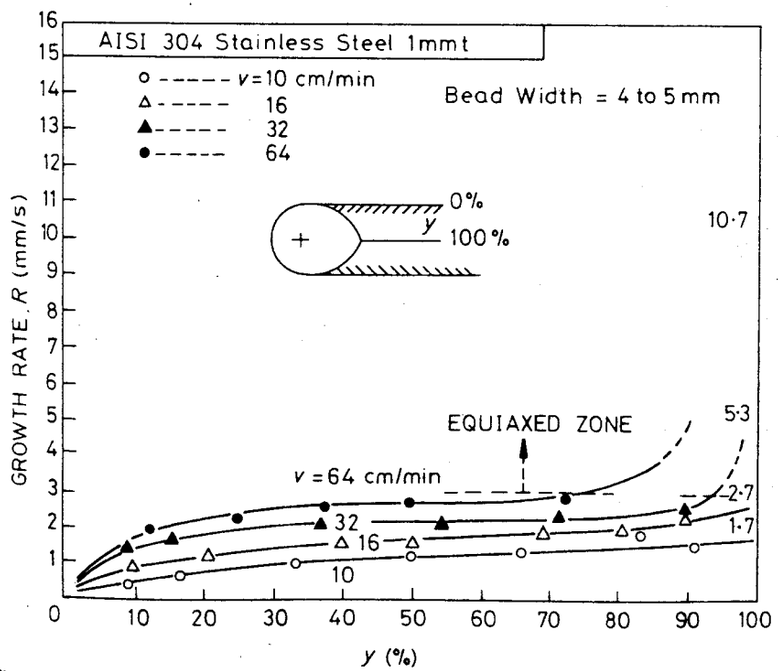

Fig. 4.52 Measurements of crystal growth rate in stainless steel as a function of per cent of weld solidified. (After T. Senda *et al.*, *Technical Report, Osaka University* **20** (1970) 932.)

While fairly linear dendritic growth is seen to predominate in this figure, it is also observed that dendrites suddenly change direction at the centre of the weld by as much as 60°. This feature of high-speed welding will now be clarified.

Geometry of Crystal Growth

Consider a welding process in which the arc is moving at a speed v. Crystal growth must occur such that it is able to keep pace with the welding speed, and this is illustrated in Fig. 4.51. It is seen that for crystal growth rate, R, to keep pace with the welding speed, v, the condition must be met that:

$$R = v \cos \theta \tag{4.49}$$

In the figure, the arrows represent vectors of speed. The vector representing the welding speed, or the speed of movement of the isotherms, is constant. On the other hand, the vector representing crystal growth rate must continuously adjust itself as growth proceeds towards the weld centre-line. It thus follows from Equation 4.49 that the solidification rate is greatest when $\theta \simeq 0$, i.e. at the weld centre-line, and lowest at the weld edge where θ is a maximum. On this basis the sudden change in crystal growth direction at the weld centre line illustrated in Fig. 4.50 is associated with high growth rates as solidification attempts to keep pace with the moving arc. In addition, the initial low rates of crystal growth are associated with a relatively planar solidification front, and as the growth rate increases, the morphology of the front changes to cellular and then cellular dendritic.

An example of weld solidification rates as measured on stainless steel as a function of different welding speeds is shown in Fig. 4.52. In confirmation of Equation 4.49, it was found that completion of weld solidification ($y = 100\%$) corresponds to the highest growth rates. However, the higher welding speeds were associated with a transition from predominantly columnar crystal growth to equiaxed growth at the final stage of solidification. This transition is thought to be due to the high amounts of segregation associated with the final stages of weld solidification. This, coupled with the shallow thermal gradient at this stage leads to high degrees of constitutional supercooling and therefore the driving force for random dendritic growth to occur is large. However, it should be noted that in general dendritic and cellular substructures in welds tend to be on a finer scale than in casting, and this is mainly due to the comparatively high solidification rates of weld metal. Since higher welding speeds or thicker base metal give larger rates of solidification, it follows that the finest substructures are associated with these welds (see Equation 4.48).

When the arc is switched off at the completion of a weld run, an elliptical molten pool is left to solidify with a comparatively shallow thermal gradient. This leads to large constitutional supercooling and marked segregation. The final substructure of these weld 'craters' is thus usually equiaxed–dendritic.

Summarizing, weld solidification has the following features:

1. Solidification initially occurs epitaxially at the melted-back grains of the base metal.
2. To begin with crystal growth is relatively slow, forming first a planar and then a fine cellular substructure.
3. The intermediate stage of crystal growth is cellular-dendritic leading to coarse columnar crystal growth in the ⟨100⟩ direction in the case of cubic crystals.
4. Final solidification at the centre-line is associated with rapid crystal growth and marked segregation. Depending on welding conditions, final dendritic structure can be equiaxed.

In many ways, therefore, weld solidification and even continuous casting exhibit essentially different features to those of ingot casting (problem 4.22).

4.6 Solidification during Quenching from the Melt

The treatment of solidification presented in this chapter has been applicable for cooling rates of less than about 10^3 K/s. However, solidification can also occur at much higher rates of $10^4 - 10^7$ K/s in such processes as liquid metal atomization, melt spinning, roller-quenching or plasma spraying, as well as laser or electron beam surface treatment. By quenching melts it is possible to achieve various metastable solid states not predicted by equilibrium phase diagrams: solid phases with extended solute solubility, new metastable crystalline phases or, if the cooling rate is fast enough, amorphous metallic glasses. Crystalline solidification can occur without microsegregation or with cells or secondary dendrites spaced much more finely than in conventional solidification processes. Whether the solid is crystalline or amorphous, rapid solidification processing offers a way of producing new materials with improved magnetic or mechanical properties.

One consequence of rapid cooling can be that local equilibrium at the solid/liquid interface breaks down. Melts can solidify with no change in composition, i.e. partitionless solidification or solute trapping can occur. The thermodynamic principles involved in partitionless solidification are similar to those for the massive transformation in solids to be treated in Section 5.9.

4.7 Case Studies of some Practical Castings and Welds

4.7.1 Casting of Carbon and Low-Alloy Steels

Typical composition ranges:

C: 0.1–1.0 wt%	carbon steels	low-alloy steels
Si: 0.1–0.4 wt%		
Mn: 0.3–1.5 wt%		
Cr: 1.0–1.6 wt%		
Ni: 1.0–3.5 wt%		
Mo: 0.1–0.4 wt%		

Casting processes: Castings, ingots, continuous casting.
Relevant phase diagrams: See Fig. 4.53.
Solidification transformations:

$$L \rightarrow \delta + L$$
$$\delta + L \rightarrow \delta + \gamma + L \quad \text{(peritectic: } \delta + L \rightarrow \gamma\text{)}$$
$$\delta + \gamma + L \rightarrow \gamma$$

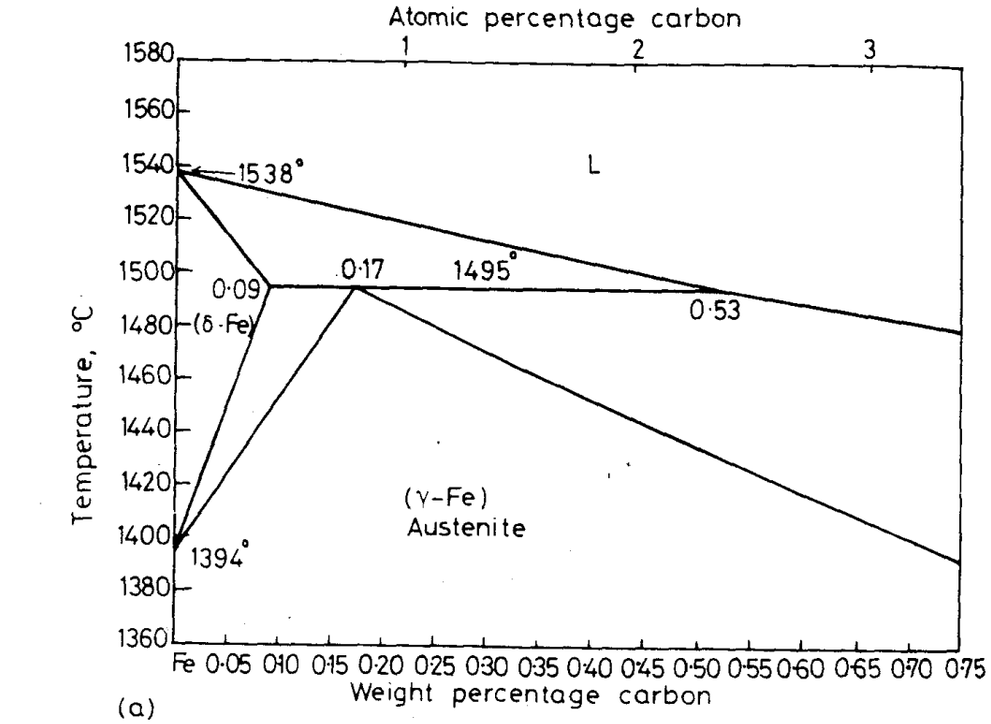

Fig. 4.53 (a) Part of the iron-carbon phase diagram. (b) Liquidus projection for the Fe–Cr–Ni system, (c) isothermal section (650 °C) for the Fe–Cr–Ni system. (From *Metals Handbook*, 8th edn., Vol. 8; American Society for Metals, 1973, pp. 276 and 425.)

Subsequent transformations:

$$\gamma \rightarrow \alpha + Fe_3C \quad \text{(equilibrium structure at ambient temperature)}$$

Microstructures: See Fig. 4.54.

Comments: Figure 4.53 shows that alloying with the relatively small amounts of Ni and Cr used in low-alloy steels has little effect on solidification temperature and that the equilibrium structure of the alloy is $\alpha(+Fe_3C)$. Figure 4.54a shows that quenching from the $(\gamma, \delta + L)$ field leaves a structure with considerable residual melt between solidified dendrites. As discussed earlier, in practical alloys, the presence of residual melt between dendrite arms is largely due to impurity segregation. The completely solidified structure shown in Fig. 4.54b exhibits a residual eutectic between α-Fe dendrites of $\gamma/Fe_3P/Fe_3C$, suggesting that the last liquid to solidify was rich in P and C. The retention of some γ-Fe in the eutectic is possibly due to the high carbon content of the residual iron (the solubility of P in γ-Fe is very low), which, together with the stabilizing effect of Ni, may help to retard the $\gamma \rightarrow \alpha$ transformation. Slower rates of cooling would probably reduce the amount of retained austenite still further. The presence of Mn induces the reaction: $Mn + S \rightarrow MnS$ (see Fig. 4.54b). However, this is certainly preferred to FeS, which tends to wet dendrite boundaries more extensively than MnS and is a prime cause of hot cracking.

4.7.2 Casting of High-Speed Steels

Typical composition ranges:

C: 0.5–1.0 wt%
Cr: 0.5–4.0 wt%
Mo: 0.5–9.5 wt%
W: 1.5–6.0 wt%
V: 0.5–2.0 wt%

Casting processes: Ingot
Special properties: Hard, tough, wear-resistent at elevated temperatures.
Relevant phase diagrams: See Fig. 4.55.
Solidification transformations:

$$L \rightarrow L + \alpha$$
$$L + \alpha \rightarrow L + \alpha + \gamma \quad \text{(peritectic } L + \delta \rightarrow \gamma\text{)}$$
$$L + \alpha + \gamma \rightarrow L + \alpha + \gamma + M_xC$$
$$L + \alpha + \gamma + M_xC \rightarrow \gamma + M_xC \quad \text{(eventually: } \rightarrow \alpha + M_xC\text{)}$$

Microstructures: See Fig. 4.56.

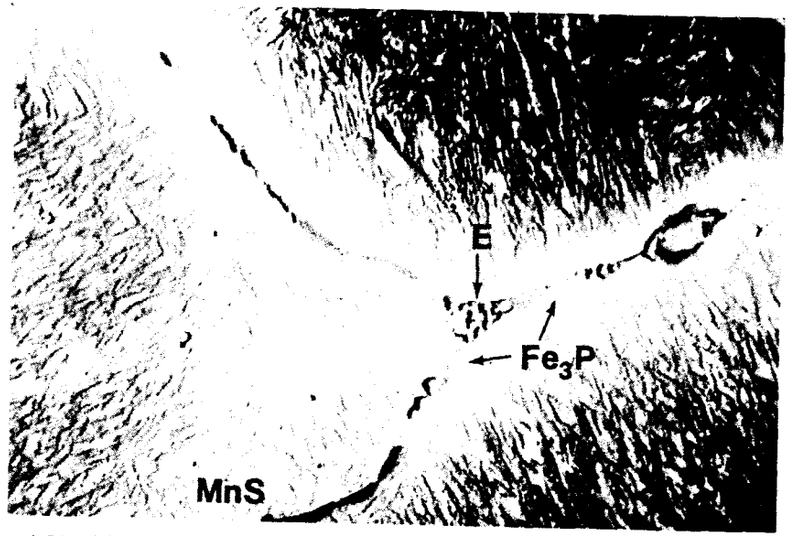

Fig. 4.54 (a) Alloy quenched from (δ, γ + L) field (× 25). (b) Cooled to 20 °C. E refers to $\gamma/Fe_3P/Fe_3C$ eutectic (× 1000). (From *Guide to the Solidification of Steels*, Jernkontoret, Stockholm, 1977.)

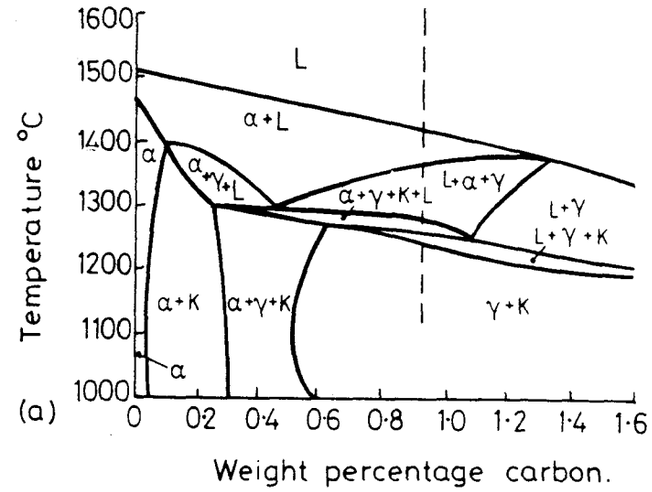

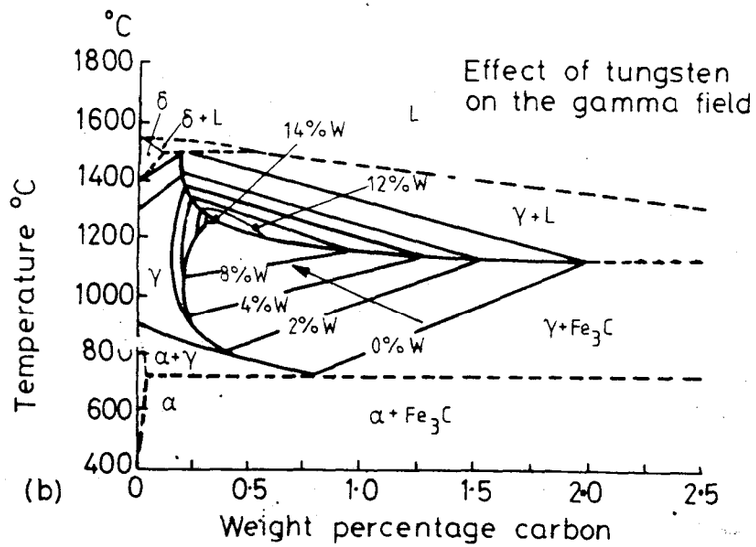

Fig. 4.55 (a) Phase diagram for steel with approx 4wt% Cr, 5wt% Mo, 6wt% W and 2wt% V (after E. Horn and H. Brandis, *DEW-Techn. Ber.* **11** (1971) 147). (b) Effect of W on γ field of steel (from *Metals Handbook*, 8th edn., Vol. 8. American Society for Metals, 1973, p. 416).

Comments: Reference to the phase diagrams (Fig. 4.55) shows that the presence of W, V and the other main alloying elements produces a cascade of polyphase fields during cooling of these castings. Solidification occurs initially with the formation of α dendrites, but the γ fields are so extensive that rapid quenching from the α + L field can not suppress the nucleation and growth of austenite (Fig. 4.56a). As expected, the C segregates strongly when α forms, but W, Cr and V are not expected to segregate so markedly in α-Fe. It seems likely that the early formation of γ through the reaction: α + L → γ + L in these castings is the main cause of the extensive segregation of W, Cr and V as observed in Fig. 4.56b and c. As seen in Fig. 4.56b, it is possible that the α → γ reaction occurs through the rejection of dissolved M back to the melt. Reference to the Fe–Cr, Fe–V, and Fe–W binary phase diagrams shows in all cases very low high-temperature solubility of these elements in γ-Fe. The resulting as-solidified structure (Fig. 4.56c) thus consists of α dendrites (following the γ → α solid-state transformation during cooling) with marked

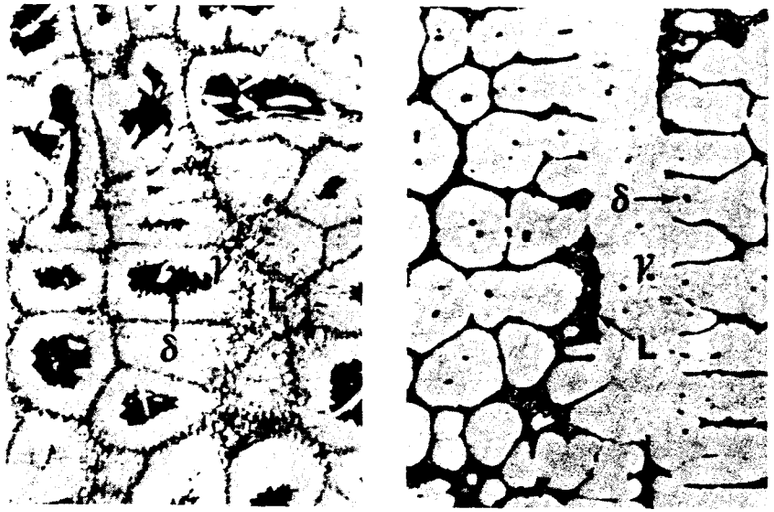

Fig. 4.56 (a) Quenched from the (L + α (or δ) + γ) field at 1335 °C (× 150). (b) Quenched from 1245 °C (× 150). (c) Same alloy after mechanical and thermal heat treatments (× 750). (a–c from *A Guide to the Solidification of Steel*, Jernkontoret, Stockholm, 1977. and d from *Metals Handbook*, 8th edn., Vol. 7, American Society for Metals, 1972, p. 121.)

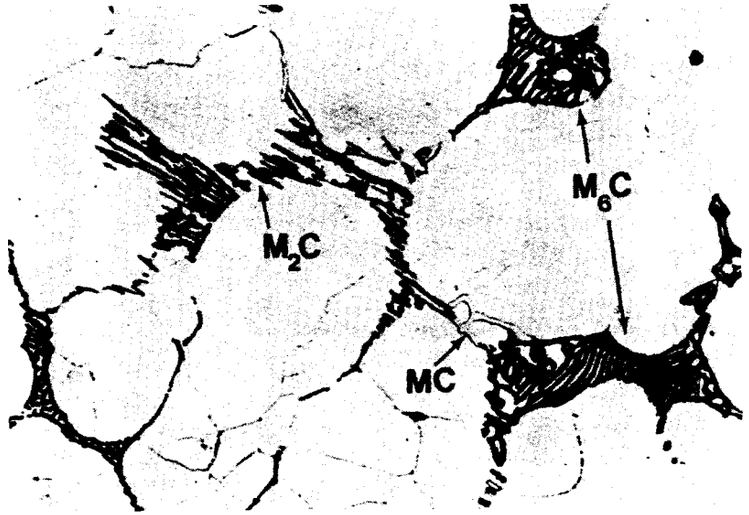

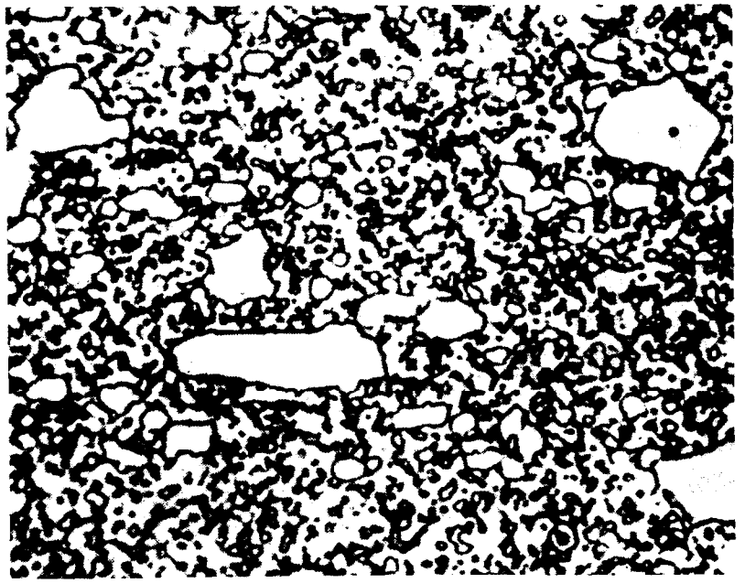

Fig. 4.56b & c (*continued*)

interdendritic segregation. The latter appears in the form of a γ/M_xC eutectic, where M_xC refers to mixed carbides of WC, Cr_2C, VC, etc. The final structure of this type of tool steel (Fig. 4.56d) is only reached after further extensive plastic working to break up the eutectic, followed by austenitizing and double-tempering treatments.

4.7.3 *Stainless Steel Weld Metal*

Electrode composition range:

Cr: 17–19 wt%
Ni: 8 –10 wt%
C: 0.05–0.1 wt%
Si: 0.5–1.0 wt%
Mn: 0.5–1.5 wt%
P: } traces
S: }

Welding process: Manual metal arc, gas metal arc.
Relevant phase diagrams: See Fig. 4.57.
Phase transformations:

$$L \rightarrow \delta + L$$
$$\delta + L \rightarrow \delta + \gamma \quad \text{(approx. peritectic)}.$$

Microstructures: See Fig. 4.58.

Comments:

(*a*) *Phase equilibria*. Figure 4.57a is the 18% Cr vertical section of the Fe–Cr–Ni ternary diagram. The effect of these and other alloying elements on the final microstructure, assuming fairly high quench rates typical of welding, can be predicted with the help of the Shaeffler diagram 4.57b. From this diagram it can be seen that if the Ni or Cr contents are reduced much below the nominal analyses given, there is a risk that martensite forms. The most important feature of these alloys with respect to welding, is that some δ-Fe is retained even at ambient temperatures (see 4.57b).

There has been much discussion in the literature as to which phase solidifies first after welding. According to Fig. 4.57a it appears that solidification should initiate with the nucleation of δ-Fe. However, if the base metal is fully austenitic at the transition zone, this phase should nucleate first because of the requirement of epitaxial growth (see previous discussion). Unfortunately the situation is complicated in practice by the presence of carbon and nitrogen, both of which tend to move the peritectic composition towards higher Ni content. An example of the effect of N being admitted to the weld pool is shown in Fig. 4.58a illustrating a single run weld which has remained fully austenitic. The result of this is fairly catastrophic, causing hot cracking at the austenite grain boundaries due to increased sulphur and phosphorus segregation in the austenite during solidification.

(*b*) *Microstructure*. It is thought that the first phase to solidify in this alloy is δ-Fe, enriched in Cr and impoverished in Ni, the tendency in either case being to stabilize the ferrite. Further cooling causes γ-Fe to nucleate in the Ni-rich liquid between the δ-Fe dendrites. With the development of this duplex γ + δ structure the peritectic reaction: $L \rightarrow \gamma + \delta$ continues to completion. Cooling of the weld metal to ambient temperature causes the γ-Fe phase to grow

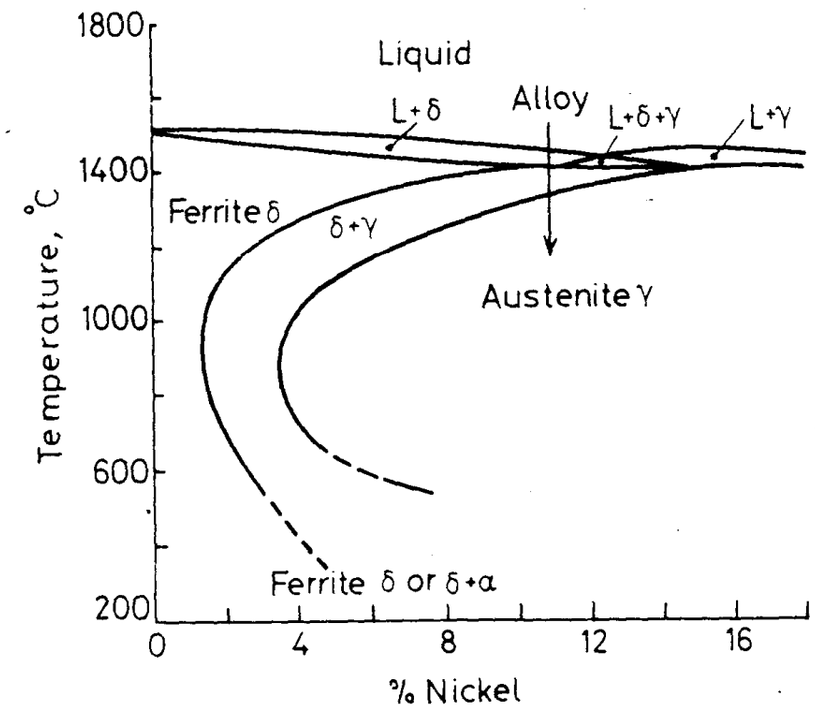

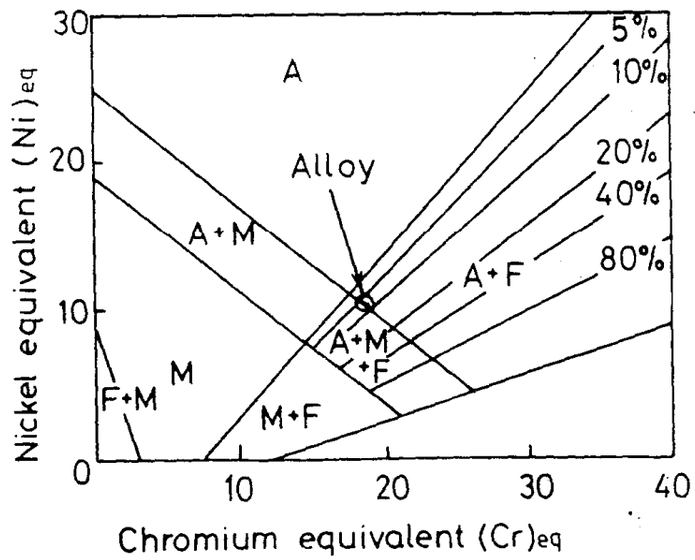

Fig. 4.57 (a) 18% Cr section of the Fe–Cr–Ni system. (b) Schaeffler diagram indicating the alloy concerned. $(NI)_{eq}$ = %Ni + 30 × %C + 0.5 × %Mn. $(Cr)_{eq}$ = %Cr + %Mo + 1.5 × %Si + 0.5 × %Nb. A, austenite; F, ferrite; M, martensite. (After R.J. Castro and J.J. de Cadenet, *Welding Metallurgy of Stainless and Heat Resistant Steels*, Cambridge University Press, Cambridge, 1974.)

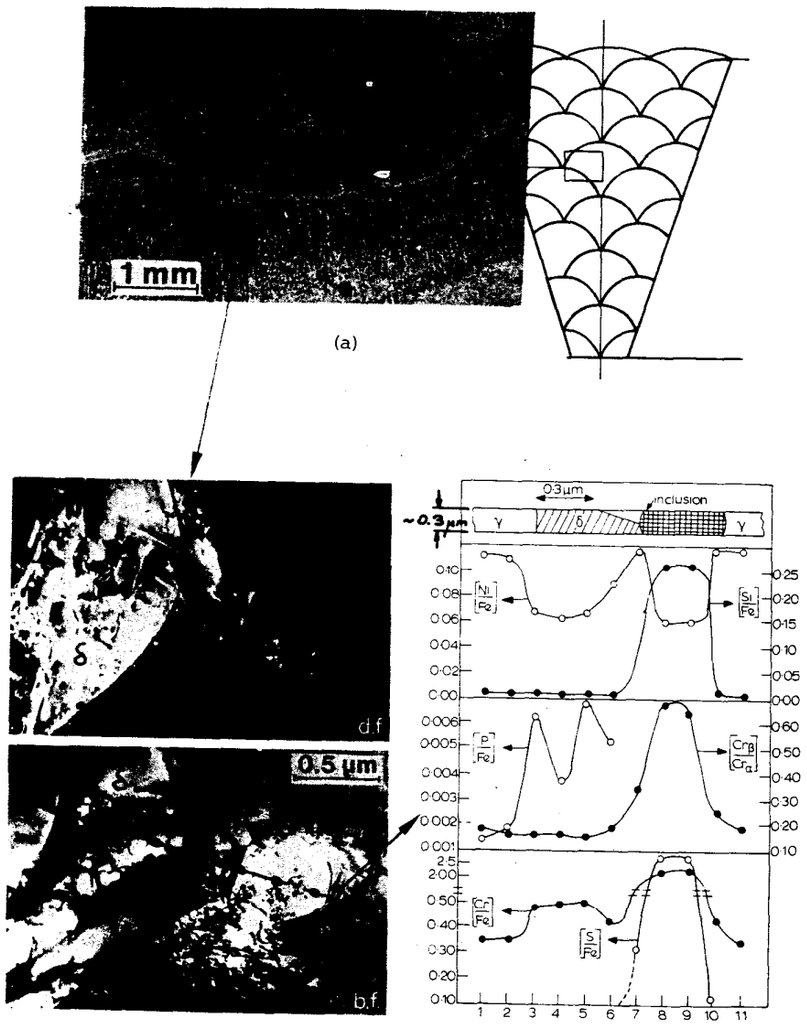

Fig. 4.58 (a) Illustrating hot cracking in the austenite region of a duplex stainless steel weld deposit. (b) STEM-EDX microanalysis of γ and δ-Fe and an inclusion. (After H. Åström *et al.*, *Metal Science Journal*, July 1976, p. 225.)

at the expense of δ-Fe until only a fine network of δ-Fe remains. The STEM-based X-ray spectrometer microanalysis of the γ, δ and inclusion phases (Fig. 4.58b) indicates that the Cr-rich ferrite has dissolved the phosphorus (one of the danger elements in hot cracking), while the sulphur is bound up in the inclusion. In this respect Mn has a double role: both as a deoxidizer and to absorb S through forming MnS. If the weld solidifies directly to γ-Fe, all the Mn remains in solution and thus cannot prevent FeS forming at cell boundaries. The fine duplex γ + δ structure of stainless steel welds thus refines and strengthens the microstructure, and effectively renders S and P harmless. It should be pointed out, however, that the 6–8 vol% retained δ-Fe at ambient temperature should not be exceeded, since higher volume fractions reduce the ductility and toughness of this alloy. In this respect, the Shaeffler diagram (Fig. 4.57b) is a useful guide for estimating δ-Fe as a function of equivalent Cr and Ni content. The amount of δ-Fe can also be measured magnetically or metallographically. If the presence of nitrogen is to be accounted for, a modified form of Shaeffler diagram (the *DeLong diagram*) can be employed (see, e.g. Castro and Cadenet, 1974)[18].

References

1. D. Turnbull and R.E. Cech, *Journal of Applied Physics*, **21**:804 (1950).
2. R.W. Cahn, *Nature*, **273**:491 (1978).
3. J. Frenkel, *Kinetic Theory of Liquids*, Dover, New York, 1955.
4. R.M.J. Cotterill *et al.*, *Phil. Mag.*, **31**:245 (1975).
5. Reasons for this crystallographic feature of dendrite growth are discussed for example in B. Chalmers, *Principles of solidification*, Wiley, 1964, p. 116.
6. V.G. Smith *et al.*, *Canadian Journal of Physics*, **33**:723 (1955).
7. W.G. Pfann, *Zone Melting*, 2nd edition, John Wiley & Sons, New York, 1966.
8. K.A. Jackson and J.D. Hunt, *Acta Metallurgica*, **13**:1212 (1965).
9. For a review of eutectic solidification see R. Elliot, 'Eutectic solidification', Review 219 in *International Metals Reviews*, September 1977, p. 161.
10. See M.C. Flemings, *Solidification Processing*, McGraw-Hill, 1974, p. 101.
11. For a complete treatment of these effects see K.A. Jackson and J.D. Hunt, *Transactions of the Metallurgical Society of AIME*, **236**:1129 (1966).
12. M.H. Burden and J.D. Hunt, 'The extent of the eutectic range', *Journal of Crystal Growth*, **22**:328 (1974).
13. F.D. Lemkey and N.J. Salkind in H.S. Peiser (Ed.), *Crystal Growth*, Pergamon, Oxford, 1967, p. 171.
14. M.C. Flemings, *Solidification Processing*, McGraw-Hill, 1974, p. 177.
15. A. Ohno, *The Solidification of Metals*, Chijin Shokan, Tokyo, 1976, p. 69.
16. For a detailed treatment see M.C. Flemings, 'Principles of control of soundness and homogeneity of large ingots', *Scandinavian Journal of Metallurgy*, **5**:1 (1976).